Tetraboride

DOI: 10.1002/anie.201306548

Peierls-Distorted Monoclinic MnB_4 with a Mn–Mn Bond**

*Arno Knappschneider, Christian Litterscheid, Nathan C. George, Jakoah Brgoch, Norbert Wagner, Johannes Beck, Joshua A. Kurzman, Ram Seshadri, and Barbara Albert**

Dedicated to Professor Hartmut Bärnighausen on the occasion of his 80th birthday

Abstract: *Tetraborides of chromium and manganese exhibit an unusual boron-atom framework that resembles the hypothetical tetragonal diamond. They are believed to be very hard. Single crystals of MnB_4 have now been grown. The compound crystallizes in the monoclinic crystal system (space group $P2_1/c$) with a structure that has four crystallographically independent boron-atom positions, as confirmed by ^{11}B MAS-NMR spectroscopy. An unexpected short distance between the Mn atoms suggests a double Mn–Mn bond and is caused by Peierls distortion. The structure was solved using group-subgroup-relationships. DFT calculations indicate Mn^I centers and paramagnetism, as confirmed by magnetic measurements. The density of states shows a pseudo-band gap at the Fermi energy and semiconducting behavior was observed for MnB_4.*

Manganese tetraboride, MnB_4, has been known to exist in the form of multiphase crystalline powders for more than 50 years.[1] It was proposed to exhibit a framework very similar to that of CrB_4,[2,3] which in turn is proposed to resemble a hypothetical tetragonal diamond.[4] Super-hardness in Mn and Cr tetraborides was also predicted.[5–9] Recently, we were able to grow single crystals of CrB_4, which contains an unusual boron-atom arrangement with distorted BB_4 tetrahedra that are corner- and edge-connected in all three dimensions. We also reported the experimental hardness,[10,11] which was then confirmed from ab initio calculations.[12] Herein, we present the first single-crystal growth, crystal-structure determination using group-subgroup relationships,[13] ^{11}B NMR spectroscopy, and electronic-structure calculations of the title compound.

MnB_4 was found to crystallize in a monoclinic structure with a short Mn–Mn contact that suggests a multiple Mn–Mn bond. According to density functional theory (DFT) calculations, the Mn–Mn pairs in the structure (here called dimerized) result from a Peierls distortion, and the manganese atoms are in an oxidation state near +I. Compounds with Mn^I are rare, example include alkali-metal hexacyanomangantes(I)[14] and manganese carbonyls (example in Ref. [15]), as well as nitridometalates like $Li_2[(Li_{1-x}Mn_x)N]$.[16]

Gray single crystals (Figure 1) and microcrystalline powders of MnB_4 were synthesized from the elements by solid-state reaction at high temperatures. According to X-ray powder diffraction (see Supporting Information), the samples are single phase. The powder pattern contains small reflections that were inconsistent with the cell parameters and the *C*-centered space group $C2/m$ published earlier for MnB_4.[2,3] Rather it can be indexed on basis of a larger primitive unit cell than originally anticipated ($a' = 2c$, $b' = -b$, $c' = a$, compared to Ref. [2,3]).[17] Group-subgroup relationships between CrB_4 and MnB_4 gave the initial parameters for a structure refinement in space group $P2_1/c$ as well as the twin law (Figure 2 and Supporting Information). The monoclinic structure of MnB_4 (Figure 3A) is characterized through a three-dimensional

Figure 1. Crystals of MnB_4.

[*] A. Knappschneider, Dr. C. Litterscheid, Prof. Dr. B. Albert
Department of Chemistry, Technische Universität Darmstadt
Alarich-Weiss-Str. 12, 64287 Darmstadt (Germany)
E-mail: albert@ac.chemie.tu-darmstadt.de
N. C. George, Dr. J. Brgoch, Dr. J. A. Kurzman, Prof. Dr. R. Seshadri
Department of Chemistry & Biochemistry, Materials Department, and Materials Research Laboratory, University of California
Santa Barbara, CA 93106 (USA)
N. Wagner, Prof. Dr. J. Beck
Institute of Inorganic Chemistry
Rheinische Friedrich-Wilhelms-Universität Bonn
53121 Bonn (Germany)

[**] Financial support by the Alexander von Humboldt foundation and the German Academic Exchange Service is gratefully acknowledged (B.A.). N.C.G. is supported by a fellowship from the ConvEne IGERT Program (NSF-DGE 0801627). The research in Santa Barbara is supported by the National Science Foundation (NSF) through DMR 1105301. Use of shared experimental facilities of the Materials Research Laboratory (MRL): an NSF MRSEC (DMR 1121053), and of the Center for Scientific Computing supported by the California Nanosystems Institute, Hewlett–Packard, and the Materials Research Laboratory, is gratefully acknowledged. The MRL is a member of the NSF-supported Materials Research Facilities Network (www.mrfn.org).

Supporting information for this article is available on the WWW under http://dx.doi.org/10.1002/anie.201306548.

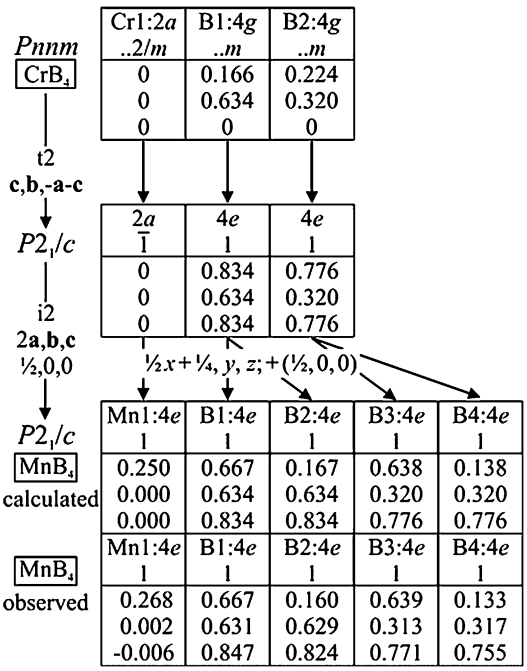

	Cr1:2*a*	B1:4*g*	B2:4*g*
	..2/*m*	..*m*	..*m*
	0	0.166	0.224
	0	0.634	0.320
	0	0	0
	2*a*	4*e*	4*e*
	$\bar{1}$	1	1
	0	0.834	0.776
	0	0.634	0.320
	0	0.834	0.776

	Mn1:4*e*	B1:4*e*	B2:4*e*	B3:4*e*	B4:4*e*
	1	1	1	1	1
	0.250	0.667	0.167	0.638	0.138
	0.000	0.634	0.634	0.320	0.320
	0.000	0.834	0.834	0.776	0.776
	Mn1:4*e*	B1:4*e*	B2:4*e*	B3:4*e*	B4:4*e*
	1	1	1	1	1
	0.268	0.667	0.160	0.639	0.133
	0.002	0.631	0.629	0.313	0.317
	-0.006	0.847	0.824	0.771	0.755

Figure 2. Group-subgroup relationships between CrB_4 and MnB_4, derived according to Ref. [13].

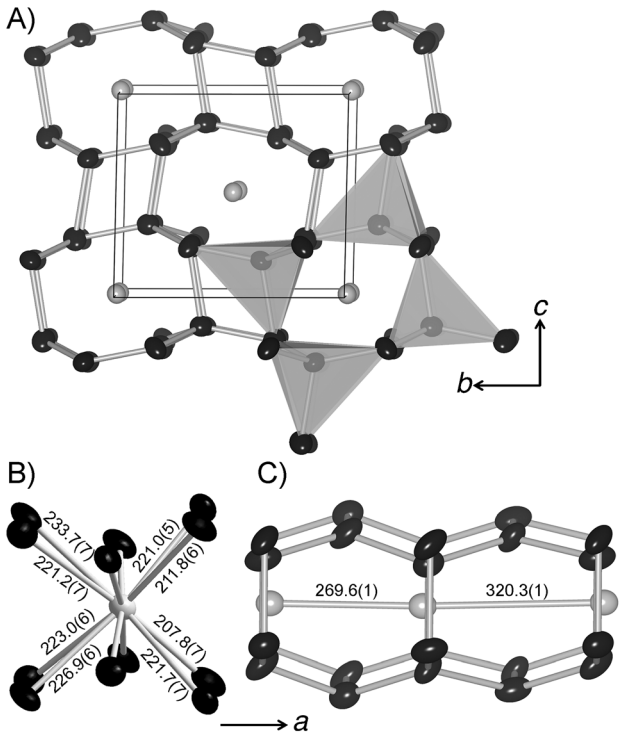

Figure 3. A) Unit cell of MnB_4, showing B black spheres, and Mn gray spheres (anisotropic ellipsoids of the displacement parameters are set at 95% probability). B) MnB_{12} coordination sphere, and c) Mn–Mn distances. Distances are given in pm.

framework of distorted BB_4 tetrahedra. Four boron atom positions were identified. The coordination environments of B1 and B2 are almost tetrahedral but B3 and B4 exhibit (3 + 1) coordination, which takes the structure far from the ideal tetragonal diamond framework previously discussed.[4] The boron framework is of covalent character and the distances are only slightly longer than typical B–B bonds. The metal atoms are almost in the center of the B_{12} cages formed from two boat-like six-rings. The displacement from the center of the cage is shown in Figure 3B, and Mn–B contacts vary between 207.8(7) pm and 233.7(7) pm. There are two metal–metal distances observed in MnB_4, 269.61(7) pm and 320.33(7) pm (Figure 3C), which is in contrast to the equally spaced metal atoms in CrB_4. Compared to diamagnetic MnP_4, which has an oxidation state of Mn^{II}, MnB_4 shows even shorter Mn–Mn distances (in MnP_4, Mn–Mn distances are greater than 292.1 pm[18]). The Mn–Mn bond in $[Mn_2(CO)_{10}]$ is also longer (292.3 pm) than the one observed in MnB_4.[19]

To understand the distortion in this compound, electronic structures were calculated based on density functional theory for the experimentally observed structure with Mn–Mn pairs (dimerized) as well as a hypothetical, "un-dimerized" structure. The density of states (DOS) for the "un-dimerized" structure model displays a large peak at the Fermi level indicating an electronic instability. Examining the band structure, it is found that the peak arises from a doubly degenerate band with $(x^2 + y^2)$ and z^2 character occurring at Γ. These bands are prone to a Peierls-type distortion that splits the degeneracy and opens up a deep pseudo gap in the DOS of the real, dimerized compound as observed in Figure 4A. Because compounds that contain a magnetic atom (such as Mn) can also electronically rearrange through a Stoner-like mechanism, the energy stabilization due to spin-polarization was also calculated. With spin-polarization, a pseudo-gap at the Fermi level (Figure 4B), with a corresponding decrease in

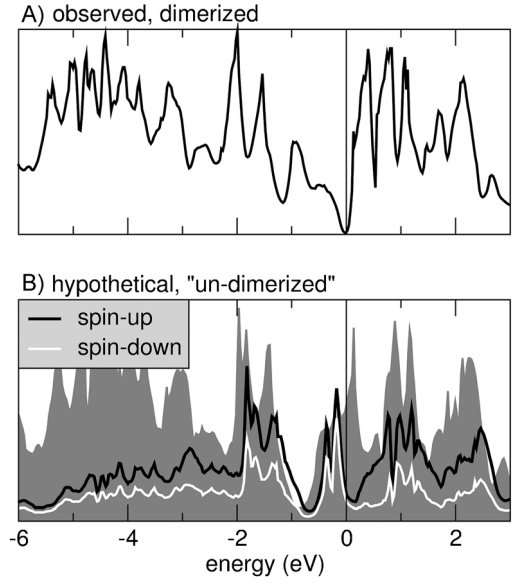

Figure 4. Densities of states of MnB_4 in the A) real, dimerized structure with a deep pseudo gap and B) hypothetical, "un-dimerized" structure (gray) that shows a maximum at E_F. The spin polarized calculation (black and white) also results in a pseudo gap, but is not favored as a result of the total energy. This situation indicates that a Peierls-like distortion with concomitant dimerization results from the electronic structure.

total energy of 145 meV per computed unit cell, is observed; however, the decrease in total energy due to Peierls-distortion is nearly two times what is observed from introducing spin-polarization; it is about 335 meV lower than the "un-dimerized" structure. The result is a breaking of the degenerate bands at Γ through a structural distortion, giving rise to the observed monoclinic structure with Mn–Mn pairs. Moreover, the monoclinic (dimerized) structure is nearly 560 meV lower in energy compared to an optimized orthorhombic MnB_4 structure, indicating the strong energy preference for the experimentally observed monoclinic structure.

Further indication of the Mn–Mn contact corresponding to a real interaction comes from an examination of the electron localization function (ELF) and crystal orbital Hamilton population (COHPs) as displayed in Figure 5 A and B. While metal–metal bonding is normally not easily identified from an ELF analysis, the total ELF in the plane containing the Mn atoms shows a distinct difference between the short and long Mn–Mn contacts. The ELF value is low but comparable to what has been identified to be a bonding Mn–Mn attraction in $Li_6Ca_2[Mn_2N_6]$.[20] The COHP (Figure 5 B) suggests significant Mn–Mn interactions in the short Mn–Mn contact. Indeed, the Mn–Mn contact in MnB_4 is short enough to be considered a double bond, consistent with expected isolobal analogy rules for d^6 Mn^I.[21] The observations made herein are in agreement with a series of recent calculations on Mn^I carbonyl compounds.[22]

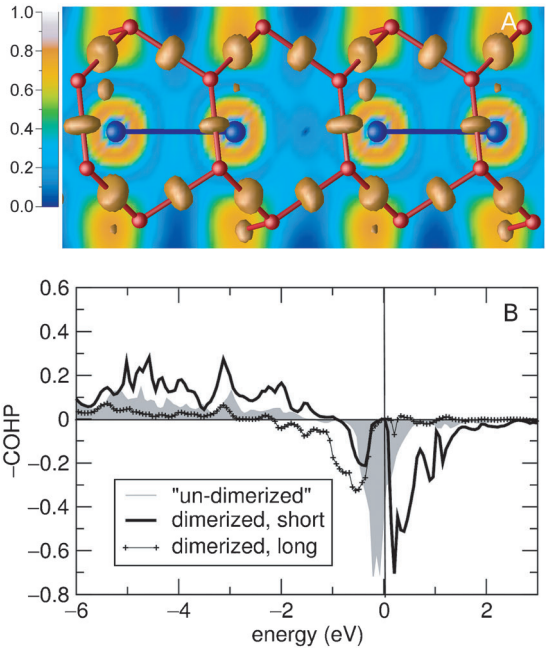

Figure 5. A) Total ELF (core + valence) contours in the plane of the Mn–Mn bond, showing slight localization within the dimers (emphasized by the blue connectors) that is absent between the dimers, that is, in the longer Mn–Mn distance. The valence-only ELF isosurface at a value of ELF = 0.80 suggests the highly localized B–B bonding in the boron framework. B) Calculated COHPs for the Mn–Mn interaction in the "un-dimerized" (hypothetical) and dimerized (experimental) structures. The large antibonding COHP at E_F is relieved by the Peierls distortion.

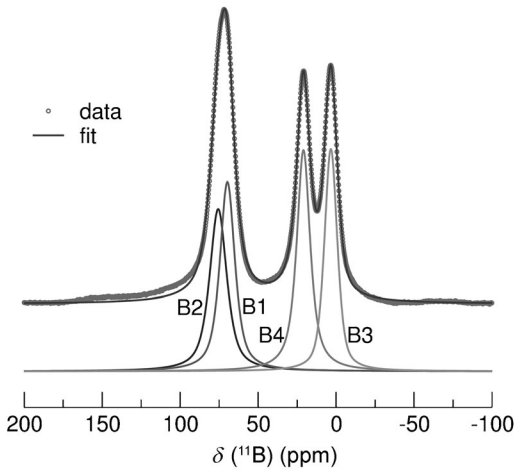

Figure 6. ^{11}B MAS NMR spectrum of MnB_4.

^{11}B NMR spectroscopy (Figure 6) did not show much sign of paramagnetic broadening or shift of the resonance signals in contrast to what has been reported for ^{11}B NMR spectra of paramagnetic iron compounds.[23] The presence of four signals in the spectrum arises from the four crystallographic independent boron atoms. Although assigning the measured peaks empirically would be impractical, the Bader charges from the DFT calculations can aid in the assignment. Such a correlation between Bader charges and NMR chemical shifts has been employed in a study of the ^{27}Al NMR spectra of aluminum oxides.[24] As given in Table 1, increasing Bader charge on a boron atom corresponds to more shielded ^{11}B nuclei, thus, resonating at lower frequency, that is, more-negative chemical shifts. The chemical shifts fall in the range of ^{11}B chemical shifts for other systems with nearly elemental boron atoms (oxidation state 0), such as in boron-doped diamond.[25] Additionally, the four B sites are present in a nearly 1:1:1:1 ratio, consistent with the crystallographic structure.

Table 1: ^{11}B NMR data.

Site	Population	Chemical shift [ppm]	FWHM[a] [ppm]	Bader charge
B1	24.8	69.6	0.30	−0.09
B2	24.4	75.6	0.30	−0.08
B3	23.6	3.3	0.47	−0.26
B4	27.2	20.9	0.18	−0.22

[a] Full width at half maximum.

The magnetic susceptibility of MnB_4 (see Supporting Information), acquired upon field-cooling under a 10 kOe field, displays a behavior that can be fitted with high certainty through the entire temperature range as the sum of a temperature-independent term χ_0 and a temperature-dependent Curie term, C/T. The value of the temperature-independent term, without accounting for sample and holder diamagnetism, is $\chi_0 = 44.6\ \mu emu\, mol^{-1}\, Oe^{-1}$, which is consistent with metallic paramagnetism. Using $\mu_{eff} = 2.84\, C^{1/2}$ in the Curie term suggests a magnetic moment near 0.64, which is the

moment that would be obtained from approximately 0.2 unpaired electrons and is consistent with a Mn^I center in a low-spin, d^6 state. The relatively small paramagnetic moment explains the absence of strong broadening of the NMR signals and the ease with which the sample could be spun in a magnetic field in the solid-state NMR experiments. The small value of μ_{eff} also explains the absence of a magnetic transition above 5 K in this compound. The absence of magnetic ordering, also suggested by an effective Weiss temperature $\Theta \approx 0$, is consistent with the small moment and the low dimensionality of the structure.

The electrical properties of MnB_4 were investigated between room temperature and 373 K using a specially designed two-probe set-up and very small crystals (edge lengths $< 100\ \mu m$). The title compound turned out to be a semiconductor with an energy of activation as low as approximately 0.04 eV, determined by an Arrhenius plot (see Supporting Information).

In conclusion, we would like to emphasize that our investigation of compounds with the hypothetical tetragonal diamond framework led to the identification of monoclinic MnB_4, which was for the first time obtained in form of crystals and pure powders. Its crystal and electronic structures allow for insights into fascinating details, such as a short Mn–Mn contact. Further experimental investigation of hardness will follow as soon as larger crystals can be grown.

Experimental Section

Manganese (279.5 mg, Aldrich, 99.99 %) and boron (222.9 mg, Chempur, 99.995 %) were mixed. A cold-pressed pellet of the starting materials was placed in a silica ampoule with freshly sublimated iodine (97 mg; Merck, double sublimated) as mineralizer. The ampoule was heated to 1273 K for 28 days (single crystals, Figure 1) or fourteen days (crystalline powders) and then quenched to room temperature. X-ray powder diffraction data were collected at room temperature using a powder diffractometer (STOE Stadi P, 1K-Mythen detector) with $CuK\alpha_1$ radiation (Ge monochromator, $\lambda = 1.54056$ Å, flat plate sample holder, transmission geometry). Single-crystal data was collected on an IPDS2 diffractometer (MoKα, Stoe, Darmstadt, Germany) at ambient temperature. The size of the MnB_4 single crystal was 0.2 mm × 0.10 mm × 0.05 mm. Structure refinement was performed using the program SHELX.[26] A numerical absorption correction was applied using X-RED and X-SHAPE software.[27] The high-resolution solid-state NMR experiments were carried out under conditions of 50 kHz magic angle spinning (MAS) at 300 K on a Bruker AVANCE IPSO NMR spectrometer, with an 11.7 T wide-bore (89 mm) superconducting magnet, operating at a frequency of 160.419 MHz for ^{11}B. A Bruker 1.3 mm H-X double-resonance MAS probe head was used with zirconia rotors and Kel-F caps. A 22.5° pulse was used to ensure quantitative measurements, with a pulse length of 2.1 μs and a recycle delay of 2 s. A total of 2560 transients were collected, and a 15 kHz line broadening was applied to the free induction decay. Chemical shifts were referenced to BF_3Et_2O at 0 ppm. The program dmfit was used to fit the NMR data.[28] The conductivity of MnB_4 was measured by the two-probe technique in a specially designed micro apparatus. A polytetrafluorethylene tube with an inner diameter of 0.6 mm was filled with several crystals. Two gold-plated pistons (diameter 0.55 mm) were inserted from both sides. The crystals were compacted by mechanical treatment and finally formed a layer of 0.1 mm thickness between the two electrodes. Conductivity was determined by applying either constant currents or constant voltages of 0.1 V. Temperature variation was achieved by external heating up to 373 K using a micro oven. Several cycles of heating and cooling and inversion of polarity were applied to the sample. Magnetic susceptibility data was acquired under a 10 kOe field while cooling under field, between 300 K and 4.2 K on a Quantum Design MPMS 5XL SQUID magnetometer. Electronic structure calculations were performed using the Vienna ab initio Simulation Package (VASP),[29,30] employing the projector-augmented wave (PAW) method[31,32] and the Perdew-Burke-Ernzerhof (PBE) generalized gradient approximation (GGA) of exchange correlation functionals.[33] Structures were optimized including volume, *c*/*a* ratio, and atomic positions to ensure that they are in their electronic ground state. Because the optimization of the hypothetical "un-dimerized" structure led to a dimerization, the positions of the Mn atoms were held static to maintain the equal (i.e., non-alternating) Mn–Mn bond lengths. Charges on Mn and B were determined by the Bader method with the aid of the Bader analysis program,[34] based on the atoms in molecules (AIM) theory.[35] The Stuttgart-LMTO-ASA program[36] was employed to calculate the crystal overlap Hamilton populations (COHP)[37] and the electron localization function (ELF).[38]

Received: July 26, 2013
Revised: September 19, 2013
Published online: January 22, 2014

Keywords: boron · conductivity · magnetism · manganese · structure elucidation

[1] R. Fruchart, A. Michel, *C. R. Hebd. Seances Acad. Sci.* **1960**, *251*, 2953 – 2954.
[2] S. Andersson, *Acta Chem. Scan.* **1969**, *23*, 687 – 688.
[3] S. Andersson, J. O. Carlsson, *Acta Chem. Scan.* **1970**, *24*, 1791 – 1799.
[4] J. K. Burdett, E. Canadell, *Inorg. Chem.* **1988**, *27*, 4437 – 4444.
[5] L. Y. Markovskii, E. T. Bezruk, *J. Appl. Chem. USSR* **1967**, *40*, 1160 – 1163.
[6] B. Wang, X. Li, Y. X. Wang, Y. F. Tu, *J. Phys. Chem. C* **2011**, *115*, 21429 – 21435.
[7] H. Niu, J. Wang, X.-Q. Chen, D. Li, Y. Li, P. Lazar, R. Podloucky, A. N. Kolmogorov, *Phys. Rev. B* **2012**, *85*, 144116.
[8] H. Gou, Z. Li, H. Niu, F. Gao, J. Zhang, R. C. Ewing, J. Lian, *Appl. Phys. Lett.* **2012**, *100*, 111907.
[9] H. B. Xu, Y. X. Wang, V. C. Lo, *Phys. Status Solidi RRL* **2011**, *5*, 13 – 15.
[10] A. Knappschneider, C. Litterscheid, J. Kurzman, R. Seshadri, B. Albert, *Inorg. Chem.* **2011**, *50*, 10540 – 10542.
[11] A. Knappschneider, C. Litterscheid, D. Dzivenko, J. Kurzman, R. Seshadri, N. Wagner, J. Beck, R. Riedel, B. Albert, *Inorg. Chem.* **2013**, *52*, 540 – 542.
[12] B. Li, H. Sun, C. Zang, C. Chen, *Phys. Rev. B* **2013**, *87*, 174106.
[13] H. Bärnighausen, *MATCH* **1980**, *9*, 139 – 175.
[14] W. D. Treadwell, W. E. Raths, *Helv. Chim. Acta* **1952**, *35*, 2259 – 2275.
[15] L. F. Dahl, C.-H. Wie, *Acta Crystallogr.* **1963**, *16*, 611 – 616.
[16] R. Niewa, F. R. Wagner, W. Schnelle, O. Hochrein, R. Kniep, *Inorg. Chem.* **2001**, *40*, 5215 – 5222.
[17] a) Space group $P2_1/c$ (no. 14), $a = 589.82(2)$, $b = 537.32(2)$, $c = 551.12(2)$ pm, $\beta = 122.633(3)°$. A whole sphere in the range $4.1 \leq \theta \leq 34.4°$ was measured. In a final step of the refinement one of the twinning laws was introduced ([−1 0 0 0 −1 0 1 0 1] corresponding to a two-fold axis along [1 0 0]). The twinning laws were derived as follows: In the "translationsgleiche" transition of index 2 from space group *Pnnm* (No. 58) to space group $P2_1/n$ (no. 14) the twofold axis along [1 0 0] and the mirror plane perpendicular to [1 0 0] are lost, but they are preserved as twinning elements in the crystal. Finally, all atoms were refined

allowing for anisotropic displacement parameters. Further details on the crystal structure investigations may be obtained from the Fachinformationszentrum Karlsruhe, 76344 Eggenstein-Leopoldshafen, Germany (fax: (+49) 7247-808-666; e-mail: crysdata@fiz-karlsruhe.de), on quoting the depository number CSD-425100; b) C. Litterscheid, A. Knappschneider, B. Albert, *Z. Anorg. Allg. Chem.* **2012**, *638*, 1608.
[18] R. Rühl, W. Jeitschko, *Acta Crystallogr. Sect. B* **1981**, *37*, 39 – 44.
[19] L. F. Dahl, R. E. Rundle, *Acta Crystallogr.* **1963**, *16*, 419 – 426.
[20] O. Hochrein, Y. Grin, R. Kniep, *Angew. Chem.* **1998**, *110*, 1667 – 1670; *Angew. Chem. Int. Ed.* **1998**, *37*, 1582 – 1585.
[21] F. G. A. Stone, *Angew. Chem.* **1984**, *96*, 85 – 96; *Angew. Chem. Int. Ed. Engl.* **1984**, *23*, 89 – 99.
[22] Z. Zhang, Q.-S. Li, Y. Xie, R. B. King, H. F. Schaefer III, *New J. Chem.* **2010**, *34*, 92 – 102.
[23] C. S. Lue, T. H. Su, B. X. Xie, S. K. Chen, J. L. MacManus-Driscoll, Y. K. Kuo, H. D. Yang, *Phys. Rev. B* **2006**, *73*, 214505.
[24] A. R. Ferreira, E. Küçükbenli, A. A. Leitão, S. de Gironcoli, *Phys. Rev. B* **2011**, *84*, 235119.
[25] M. Murakami, T. Shimizu, M. Tansho, Y. Takano, S. Ishii, E. A. Ekimov, V. A. Sidorov, K. Takegoshi, *Physica C* **2010**, *470*, S625 – S626.
[26] G. M. Sheldrick, *Acta Crystallogr. Sect. A* **2008**, *64*, 112 – 122.
[27] a) Stoe & Cie (**2009**). X-AREA, X-RED. Stoe & Cie, Darmstadt, Germany; b) Stoe & Cie (**2009**). X-SHAPE. Stoe & Cie, Darmstadt, Germany.
[28] D. Massiot, F. Fayon, M. Capron, I. King, S. Le Calvé, B. Alonso, J.-O. Durand, B. Bujoli, Z. Gan, G. Hoatson, *Magn. Reson. Chem.* **2002**, *40*, 70 – 76.
[29] G. Kresse, J. Hafner, *Phys. Rev. B* **1993**, *48*, 13115 – 13118.
[30] G. Kresse, J. Furthmüller, *Phys. Rev. B* **1996**, *54*, 11169 – 11186.
[31] P. E. Blöchl, *Phys. Rev. B* **1994**, *50*, 17953 – 17979.
[32] G. Kresse, D. Joubert, *Phys. Rev. B* **1999**, *59*, 1758 – 1775.
[33] J. P. Perdew, K. Burke, M. Ernzerhof, *Phys. Rev. Lett.* **1996**, *77*, 3865 – 3868.
[34] G. Henkelman, A. Arnaldsson, H. Jónsson, *Comput. Mater. Sci.* **2006**, *36*, 354 – 360.
[35] R. F. W. Bader, *Atoms in Molecules: A Quantum Theory*, Oxford University Press, Oxford, **1990**.
[36] O. Jepsen, O. K. Andersen, *Z. Phys. B* **1995**, *97*, 35 – 47.
[37] R. Dronskowski, P. E. Blöchl, *J. Phys. Chem.* **1993**, *97*, 8617 – 8624.
[38] A. D. Becke, K. E. Edgecombe, *J. Chem. Phys.* **1990**, *92*, 5397 – 5403.

